Published in final edited form as:
*Mol Phys*. 2012 August ; 110(15-16): 1927–1932. doi:10.1080/00268976.2012.695028.

# Multicolor stimulated Raman scattering (SRS) microscopy

**Fa-Ke Lu**, **Minbiao Ji**, **Dan Fu**, **Xiaohui Ni**, **Christian W. Freudiger**, **Gary Holtom**, and **X. Sunney Xie***
Department of Chemistry and Chemical Biology, Harvard University, Cambridge, Massachusetts 02138, United States

## Abstract

Stimulated Raman scattering (SRS) microscopy has opened up a wide range of biochemical imaging applications by probing a particular Raman-active molecule vibrational mode in the specimen. However, the original implementation with picosecond pulse excitation can only realize rapid chemical mapping with a single Raman band. Here we present a novel SRS microscopic technique using a grating-based pulse shaper for excitation and a grating-based spectrograph for detection to achieve simultaneous multicolor SRS imaging with high sensitivity and high acquisition speeds. In particular, we used linear combination of the measured $CH_2$ and $CH_3$ stretching signals to map the distributions of protein and lipid contents simultaneously.

### Keywords

coherent Raman scattering; stimulated Raman scattering; multicolor; grating; pulse shaper; lock-in; polystyrene; poly(methyl methacrylate); mouse skin; protein; lipid

## 1. Introduction

Stimulated Raman scattering (SRS) microscopy has been developed as a powerful tool for label-free chemical imaging with high chemical specificity and high acquisition speeds up to video rate [1–10]. In SRS microscopy, the sample is coherently excited by two lasers: one is the pump beam with the frequency of $\omega_p$ and the other is the Stokes beam with the frequency of $\omega_S$. When the beat frequency $\Delta\omega = \omega_p - \omega_S$ is equal to a particular Raman-active molecular vibration of the sample, SRS signals, including both stimulated Raman loss (SRL) and stimulated Raman gain (SRG), is generated due to the nonlinear interaction between the photons and the molecules [11]. SRS is free from the nonresonant background, exhibits identical spectrum as spontaneous Raman, and is linearly proportional to the concentration of the analyte, and therefore allows quantification with SRS straightforward. All of these make SRS to be a more desirable analytical tool than CARS [12].

In the original implementation of SRS microscope, two transform-limited picosecond (ps) lasers with narrow spectral bandwidth are used to excite a single Raman-active vibrational mode for fast imaging with high spectral resolution [5]. However, with this ps-ps excitation scheme, other vibrational modes of the sample are not excited, which fails to utilize the full advantage of the rich Raman spectroscopic information and therefore it is not possible to distinguish mixed chemical species with overlapped Raman bands in the sample. For quantitative analysis, such as the concentration ratios between different chemical compounds, multicolor imaging with multiple chemical contrasts is highly desirable. Furthermore, simultaneous mapping of different chemical species in the same sample is

*Corresponding author, xie@chemistry.harvard.edu.

extremely important for the investigation of co-distribution or dynamic correlation between pairs of biomolecules in many in vivo biological and biomedical applications [13]. In addition, since the cross phase modulation signal and two-color two-photon absorption (TPA) from pigments or blood may exist as a global non-Raman background in SRS, additional contrast away from any Raman resonance is mandatory in order to remove the background for acute quantitative investigations [14].

To image different Raman modes of the sample, a simple way is to tune the frequency of the pump beam or the Stokes beam in sequential scans [15]. However, this wavelength tuning approach may lose the colocalization information of different Raman modes, especially when the sample is in a dynamic environment. Spectrally tailored excitation SRS (STE-SRS) microscopy realized highly specific imaging of a particular chemical species in the presence of interfering species by spectral modulation of a broadband pump beam at a high frequency, allowing detection of the SRS signals of the narrowband Stokes beam with high sensitivity [16]. However, with this method, only one chemical contrast is obtained for each scanning. To image other chemical species, another unique mask has to be designed and used for the accordingly spectral manipulation. Multiplex SRS microscopy with double-modulation and double-demodulation approach based on a multichannel acousto-optical tunable filter (AOTF) device realized multicolor imaging with multiple chemical contrasts for quantitative determination of different chemical species [17]. Unfortunately, the scanning speed is limited by the secondary frequency modulation and demodulation procedure.

In this paper, we present a multicolor SRS microscopic imaging technique with the integration of grating-based spectral manipulation and grating-based spectrographic detection. Using this approach, multicolor images with highly specific multiple chemical contrasts are acquired in parallel with high acquisition speeds (typically ~1.2 second per frame of a 512×512 image). A narrowband ps laser (Stokes beam) and a broadband femtosecond (fs) laser source (pump beam) are synchronized. The fs beam is spectrally tailored into a comb-shape spectrum with a few narrowband peaks using a grating-based pulse shaper. The Stokes beam is amplitude modulated at a high frequency (~10MHz). A grating-based spectrograph in the detection path after the condenser is used to disperse the several peaks into different directions. The SRL signal in each spectral peak of the pump beam is measured by an independent photodiode followed by a phase-sensitive lock-in amplifier. We demonstrate the technique by imaging the mixture of polystyrene (PS) and poly(methyl methacrylate) (PMMA) beads. Using linear combination of the measured $CH_2$ and $CH_3$ stretching signals, we were able to map the distributions of protein and lipid contents simultaneously in the mouse ear skin tissue.

## 2. Experiments

The experimental setup for the multicolor SRS microscopy is shown in Figure 1. A broadband fs Ti:Sapphire laser source (Mira 900D, Coherent Inc.) is synchronized to a narrowband ps Nd:YVO4 laser (High-Q, picoTRAIN) with a Synchrolock system (Coherent Inc.). The broadband fs laser beam (700mW, FWHM ~18 nm) is delivered into a reflection-configured grating-based pulse shaper [16, 18]. An opaque amplitude mask with pre-designed triangular multi-slits is placed on the focal plane of the spectrum dispersed by the grating (inset of Figure 1) to generate a comb-shape spectrum with multi-narrowband peaks. The horizontal position of the slit determines the central wavelength of each peak, while the width of the slit determines the spectral bandwidth and the average optical power of each peak. By adjusting the height of the mask, a balance between the bandwidth and the power of each peak can be achieved. Alternatively, a liquid crystal spatial light modulator (SLM) can be used for convenient adjustment of different spectral patterns [16]. In our experiment,

up to 3 spectral peaks are used. The comb-shape spectrum (pump beam) is collinearly combined with the synchronized ps laser beam (Stokes beam) on a dichroic mirror and delivered into a modified laser scanning microscope (FV300, Olympus). The ps laser pulses at 1064 nm are amplitude modulated by the electro-optic modulator (EOM) with a polarizer at high frequency (~10MHz). In the detection part, another grating is used to spatially disperse the three peaks, which are collected by a cylindrical lens and detected by a photodiode array, followed by home-made lock-in amplifiers for multicolor SRL detection [2]. No optical blocking filter is needed because the Stokes beam at 1064 nm is diffracted into a much larger angle compared with the multi-peaks in the pump beam.

In a typical laser-scanning microscope, two-dimensional (2D) imaging is often realized through the beam scanning with 2D galvo mirrors. However, in our setup the scanning of the laser beam with large amplitude along the spectral dispersion direction may result in the spatial crosstalk among the adjacent channels, thus limiting the effective imaging field of view. We resolved this problem by replacing the 2D beam scanning with a strip scanning method: motorized sample stage is moving along the spectral dispersion direction at a constant speed, while the beam is scanning along the perpendicular direction in the line-scan mode. The motion of the beam in one direction was minimized by a cylindrical lens and therefore there is no effect on the imaging quality. The whole system is synchronized and operated by Labview programming. For mosaic laser confocal imaging, strip scanning method is three times as fast as the traditional 2D scanning [19].

## 3. Results

Figure 2(a) shows the spectra of the fs laser pulse before and after passing through the grating-based pulse shaper. Three narrowband peaks are obtained. Note that there is no sidelobe or crosstalk features between The central frequencies of the three peaks are selected to detect the corresponding Raman shift of interest. The bandwidth of the peaks determines the spectral resolution of our system. In principle, the narrower the bandwidth, the higher spectral resolution of SRS chemical selective imaging we could be able to achieve. However, narrowing bandwidth means lowering optical power. In our experiment, we balance the spectral resolution (~10–20 $cm^{-1}$) and the average power (~8–15 mW for each peak on the sample). We first characterized our system by imaging the mixture of 6-μm polystyrene (PS) beads and 1–5 μm poly(methyl methacrylate) (PMMA) beads spin coated on a cover glass. The spontaneous Raman spectra of the two types of beads are shown in Figure 2(b), with the three pre-selected bands indicated by the color bars, and their corresponding SRS images in Figures 2(c–e). In Figure 2(c), at 3054 $cm^{-1}$, only PS beads produce strong signals, while PMMA beads are almost invisible, as proved by the line intensity profile in Figure 2(g); in Figure 2(d), at 2950 $cm^{-1}$, only PMMA beads are visible (Figure 2(h)); and in Figure 2(f), at 2900 $cm^{-1}$, both of the beads are visualized. Figure 2(e) is the overlay of Figures 2(c, d), which matches well with Figure 2(f), confirmed by the line profiles as shown in Figures 2(i, j). These representations could be straightforward explained by the characteristic Raman intensities of PS and PMMA at the three frequencies as shown in Figure 2(b). Further quantitative analysis is also possible to distinguish pure chemical species from the mixed analyte. These results validate the multi-contrast capability and chemical specificity of our system. In addition, it is worthy of note that since the three-color images are acquired simultaneously, this approach provides perfect colocalized information from the specimen, even though some parts of the sample may move during imaging.

Since SRS exhibits linear concentration dependence, it is possible to quantitatively distinguish different chemical species with overlapped Raman bands, supposing that each chemical species has characteristic Raman features and the calibration data from each pure

species are available. In a mixture of $m$ chemical species, the detected multicolor SRS signals from $n$ channels ($S_n$) can be expressed as,

$$S_n=\sum_{m=1}^{M} c_m \cdot k_{m,n}, k_{m,n}=a \cdot \int \sigma_{m,n}(\omega_{p,n}-\omega_S) \cdot E(\omega_{p,n}) \cdot E(\omega_S) d\omega_{p,n} d\omega_S, \quad (1)$$

where $c_m$ and $\sigma_{m,n}$ are the concentration and the Raman cross section of a particular chemical species within a certain channel for multicolor imaging, respectively. $m$ as an integer from 1 to $M$, denotes different chemical species, while $n$ as an integer from 1 to $N$, denotes different channels. $\omega_p$ and $\omega_S$ are the pump and Stokes optical fields. $\alpha$ is a constant. The bundled parameter $k_{m,n}$ is equal to the integration of the Raman cross section and the excitation optical fields. For simplicity, we define a matrix associated with $k_{m,n}$ as below,

$$T=\begin{bmatrix} k_{1,1} & k_{2,1} & \cdots & k_{M,1} \\ k_{1,2} & k_{2,2} & \cdots & k_{M,2} \\ \vdots & \vdots & \cdots & \vdots \\ k_{1,N} & k_{2,N} & \cdots & k_{M,N} \end{bmatrix}, \quad (2)$$

and therefore the concentration of $m$ chemical species can be calculated with the following equation.

$$\begin{bmatrix} c_1 \\ c_2 \\ \vdots \\ c_M \end{bmatrix} = T^{-1} \cdot \begin{bmatrix} S_1 \\ S_2 \\ \vdots \\ S_N \end{bmatrix}, \quad (3)$$

where $T^{-1}$ is the inverse matrix of $T$, which can be directly measured for pure chemical species with our system to serve as the calibration data. From Equations (1–3), it is clear that with $N$-color SRS imaging, $M$ chemical species could be retrieved quantitatively, when $N=M$. Note that with $N>M$, overdetermined system will improve the detection sensitivity.

We use the linear combination of signals at different vibrational frequencies for quantitative multicolor tissue imaging. Figures 3(a) and (b) show the simultaneous SRS images of mouse ear skin at 2940 $cm^{-1}$ and 2845 $cm^{-1}$, corresponding to $CH_3$ stretching vibration for protein-rich mapping and $CH_2$ stretching vibration for lipid-rich mapping, respectively [20]. However, as shown in Figure 3(c), lipid and protein have severe Raman band overlapping, indicating that the chemical specificity in Figures 3(a) and (b) are poor. Based on Equations (1–3), with two-color SRS images and the pure protein and lipid calibration data, protein ($[c]_{protein} \propto 5.2S_1 - 4.16S_2$) and lipid ($[c]_{protein} \propto 1.2S_2 - 0.3S_1$) in the tissue could be quantitatively retrieved with high chemical selectivity, as shown in Figures 3(d) and (e), respectively. In the protein channel (Figure 3(d)), the hair, which is protein-rich, generates stronger signals, while in the lipid channel (Figure 3(e)), the signal from the aggregated lipids surrounding the hair, secreted by the sebaceous gland, is much stronger than from the hair itself. Figure 3(f) is the composite image of the skin protein (red) and lipids (green), which clearly reveals their relative spatial distributions. From the intensity profile across the line indicated in Figure 3(f) as shown in Figure 3(g), protein and lipid have been clearly distinguished with linear combination calculation. Figure 3(h) shows the reconstructed three-color image of the skin sample at a deeper depth (~50 μm). Condensed fat cells are visualized, between which there are protein-rich network structures. Note that the third-color image at 2780 $cm^{-1}$ corresponding to the non-Raman background (magenta bar in Figure 3(c)) is applied to detect the two-color TPA signals from blood (magenta). These TPA

signals will appear in all of the three channels, making it very convenient to be removed through digital background subtraction. Simultaneous three-color SRS imaging of skin provides the co-distribution of different chemical species, which may become a valuable tool for the quantitative study of dermatologic diseases, or for real-time monitoring drug delivery efficiency to the skin [21, 22].

## 4. Discussion and conclusion

In this paper we present a multicolor SRS microscopic imaging technique. Multicolor imaging at a few particular Raman vibrational resonances of interest is acquired simultaneously, and pure chemical species are quantitatively retrieved with linear combination calculation. This method possesses several advantages. First of all, simultaneous acquisition of multicolor images ensures the exact colocalization or relative spatial distribution of different Raman oscillators across the sample. Secondly, since different channels are working in parallel independently, there is no additional limit on scanning speed for label-free SRS imaging, which allows rapid imaging. Third, in our experiment, strip scanning method is used. For 2D mosaic imaging, this method is superior because of the absence of intensity heterogeneity in the stage moving direction compared with the traditional square tiling method [19]. As another advantage, along the stage scanning direction, strip scanning, up to one centimetre, could be readily realized with much fast acquisition speed (data not shown)..

Note that the number of the multicolor channels is extendable, but is limited by two factors: one is the restricted spectral bandwidth of the fs laser source, and the other is the limited channels in the lock-in amplifier due to its high cost to date. More channels provide more chemical contrasts from the same specimen, and in the extreme case, realized with a high density photodiode and lock-in amplifier array, the full SRS spectra with high sensitivity could also be acquired in parallel, which may play a more important role in biological and biomedical applications compared with narrowband imaging. Alternatively, with several synchronized picosecond optical parametric oscillators (OPOs) or optical parametric amplifiers (OPAs), instead of the spectrally tailored fs laser source, the spectral resolution of each peak could be dramatically improved to 3~5 $cm^{-1}$. We applied our system to image the freshly excised mouse ear skin, but for too thick tissue samples with high heterogeneity, multi-scattering may cause crosstalk between the adjacent detectors, which remains one limitation of the technique at the current stage. Although the power on the sample in our method is relatively higher than the single color imaging, we did not observe clear photobleaching or photodamag with the power we used in our experiment.

In conclusion, we demonstrate a simultaneous multicolor SRS microscopic technique with a grating-based pulse shaper for excitation and grating-based spectrograph for detection for tissue imaging and quantitative retrieval of different chemical species with multiple chemical-selective contrasts. In particular, this technique can be used for multi-parametric SRS flow cytometer, in which simultaneous detection is mandatory. It is expected that with increased channels and improved spectral resolution, this technique could find more applications in complex and important biological and biomedical systems.

## Acknowledgments

We thank Zhibo Wang and Xu Zhang for their help on the mouse tissue sample preparation, and Terumasa Ito and Wenlong Yang for technical discussions. This work was supported by the U.S. Department of Energy's Basic Energy Sciences Program (DE-SC001548) and the National Institute of Health’s T-R01 (1R01EB010244-01) awarded to X.S.X.

## References


1. Freudiger CW, Min W, Saar BG, Lu S, Holtom GR, He C, Tsai JC, Kang JX, Xie XS. Science. 2008; 322:1857. [PubMed: 19095943]
2. Saar BG, Freudiger CW, Reichman J, Stanley CM, Holtom GR, Xie XS. Science. 2010; 330:1368. [PubMed: 21127249]
3. Andresen ER, Berto P, Rigneault H. Opt. Lett. 2011; 36:2387. [PubMed: 21725420]
4. Beier HT, Noojin GD, Rockwell BA. Opt. Express. 2011; 19:18885. [PubMed: 21996830]
5. Folick A, Min W, Wang MC. Curr. Opin. Genet. Dev. 2011; 21:585. [PubMed: 21945002]
6. Frostig H, Katz O, Natan A, Silberberg Y. Opt. Lett. 2011; 36:1248. [PubMed: 21479047]
7. Gambetta A, Kumar V, Grancini G, Polli D, Ramponi R, Cerullo G, Marangoni M. Opt. Lett. 2010; 35:226. [PubMed: 20081976]
8. Liu Q, Ouyang Z, Albin S. Opt. Express. 2011; 19:4795. [PubMed: 21369311]
9. Ozeki Y, Kitagawa Y, Sumimura K, Nishizawa N, Umemura W, Kajiyama S, Fukui K, Itoh K. Opt. Express. 2010; 18:13708. [PubMed: 20588505]
10. Yakovlev VV, Noojin GD, Denton ML, Rockwell BA, Thomas RJ. Opt. Lett. 2011; 36:1233. [PubMed: 21479040]
11. Shen, YR. The principles of nonlinear optics. New York: J. Wiley; 1984.
12. Min W, Freudiger CW, Lu S, Xie XS. Annu. Rev. Phys. Chem. 2011; 62:507. [PubMed: 21453061]
13. Saar BG, Zeng Y, Freudiger CW, Liu YS, Himmel ME, Xie XS, Ding SY. Angew. Chem. 2010; 49:5476. [PubMed: 20589818]
14. Tian P, Warren WS. Opt. Lett. 2002; 27:1634. [PubMed: 18026525]
15. Slipchenko MN, Chen H, Ely DR, Jung Y, Carvajal MT, Cheng JX. Analyst. 2010; 135:2613. [PubMed: 20625604]
16. Freudiger CW, Min W, Holtom GR, Xu BW, Dantus M, Xie XS. Nature Photonics. 2011; 5:103. [PubMed: 23015809]
17. Fu D, Lu F, Zhang X, Freudiger CW, Pernik DR, Holtom GR, Xie XS. J. Am. Chem. Soc. 2012; 134:3623. [PubMed: 22316340]
18. Lu F, Zheng W, Lin J, Huang ZW. Appl. Phys. Lett. 2010; 96:133701.
19. Abeytunge S, Li YB, Larson B, Toledo-Crow R, Rajadhyaksha M. J. Biomed. Opt. 2011; 16:050504. [PubMed: 21639560]
20. Saar BG, Johnston RS, Freudiger CW, Xie XS, Seibel EJ. Opt. Lett. 2011; 36:2396. [PubMed: 21725423]
21. Saar BG, Contreras-Rojas LR, Xie XS, Guy RH. Mol. Pharm. 2011; 8:969. [PubMed: 21548600]
22. Zhang D, Slipchenko MN, Cheng JX. J. Phys. Chem. Lett. 2011; 2:1248. [PubMed: 21731798]

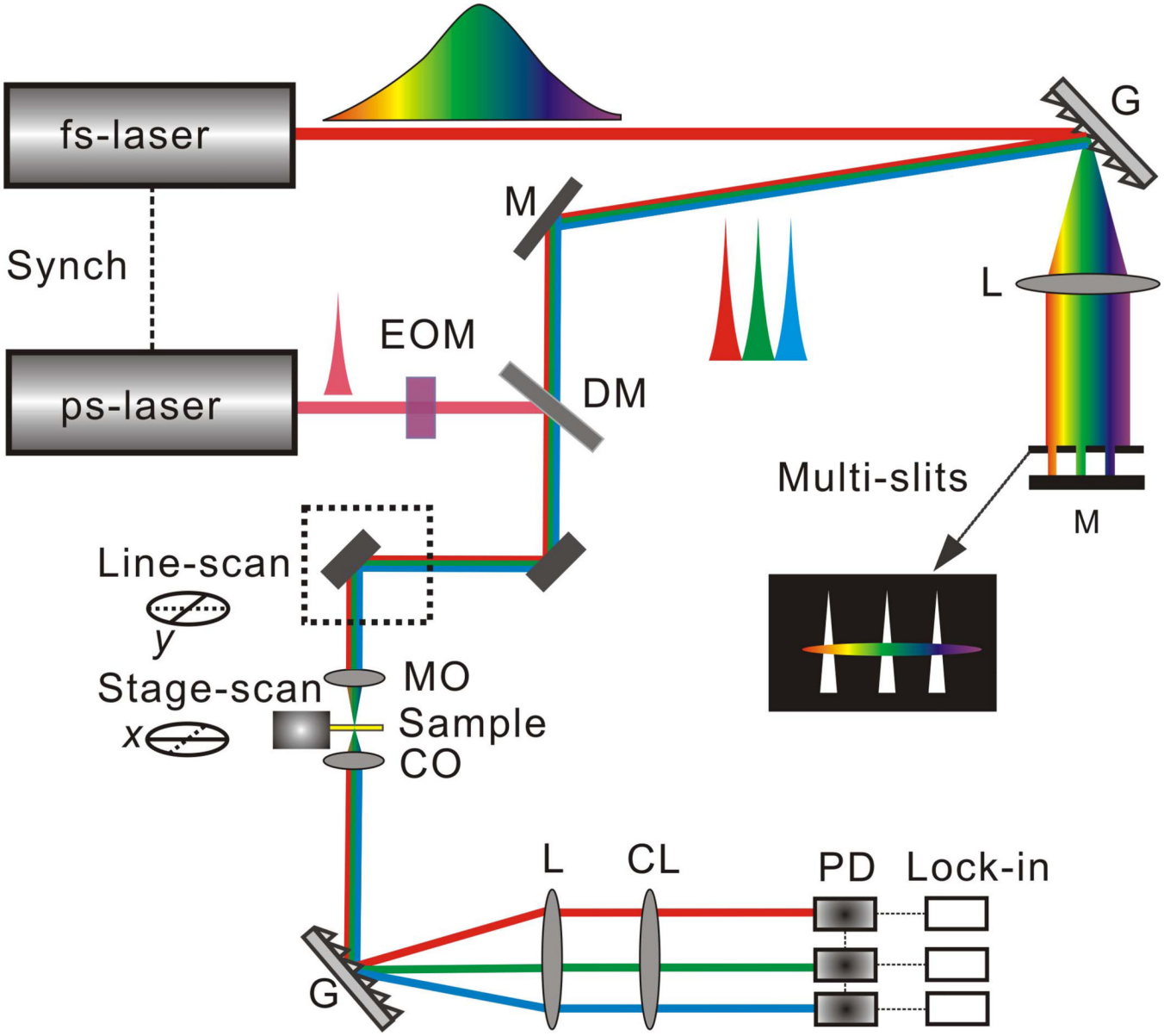


**Figure 1.**

Schematic of the experimental setup for the simultaneous multicolor SRS microscopy. A broadband femtosecond (fs) laser source is synchronized to a narrowband picosecond laser. The fs pulse is tailored into a comb-shape spectrum with multi-peaks using a grating-based pulse shaper, each of which is corresponding to a particular Raman-active molecular vibrational frequency. A grating-based spectrograph scheme is used to disperse the multi-peaks into different directions and the SRL signals are detected by a homemade photodiode array with parallel lock-in demodulators. G: grating; CL: cylindrical lens; L, lens; M: mirror; DM: dichroic mirror; EOM: electro-optic modulator; MO: microscopic objective; CO: condenser; PD: photodiode.

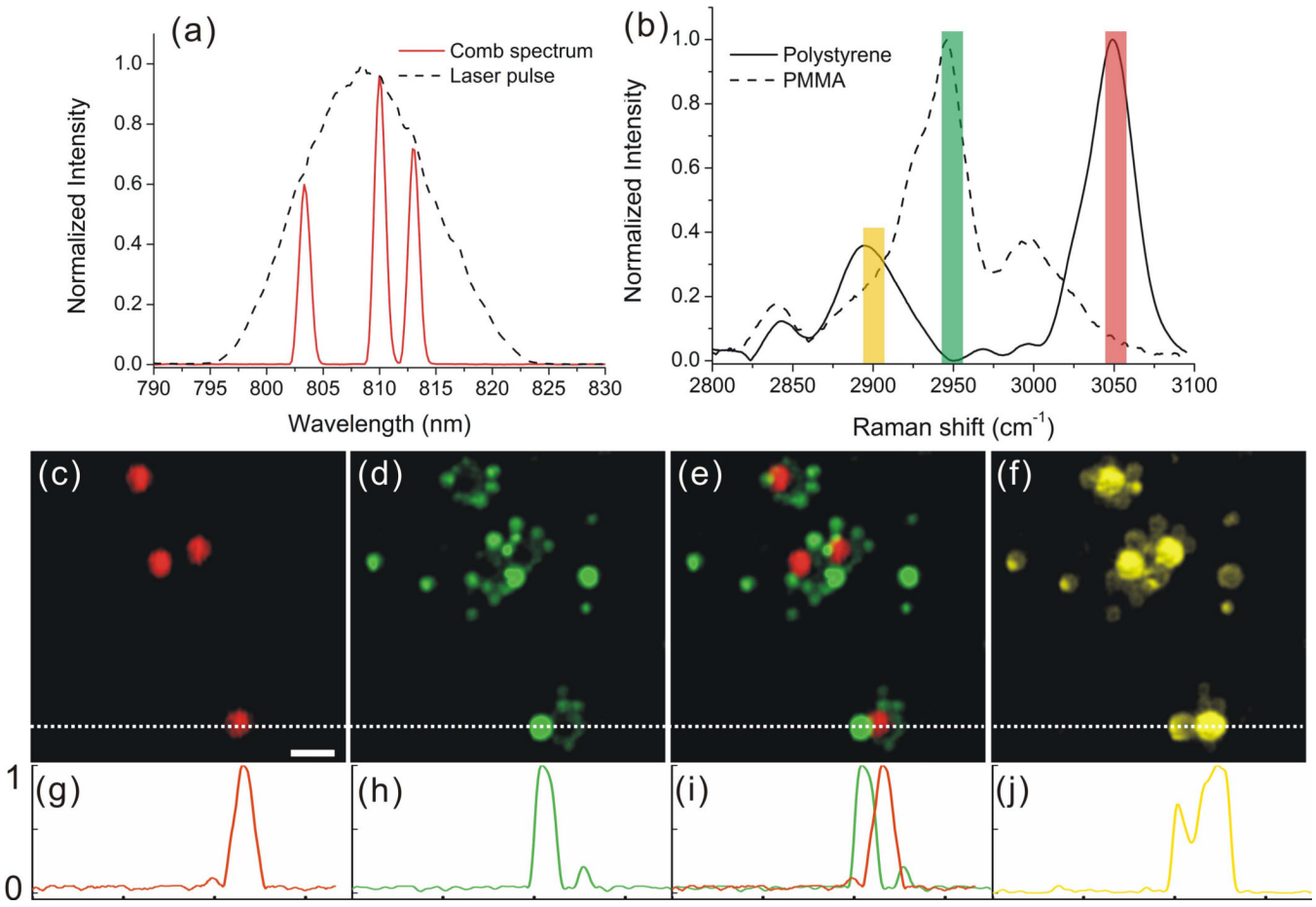


**Figure 2.**

(a) Representative spectra of the femtosecond laser pulse before and after the grating-based pulse shaper. (b) Raman spectra of the polystyrene (PS) and poly(methyl methacrylate) (PMMA). The color bars indicate the Raman frequencies selected for the simultaneous three-color imaging of mixed 6 μm PS and 1–5 μm PMMA beads as shown in Figures (c–f). (c) At 3054 $cm^{-1}$, only PS beads produce strong SRS signals (red). (d) At 2950 $cm^{-1}$, only PMMA beads are visible (green). (f) At 2900 $cm^{-1}$, both PS and PMMA beads are visible (yellow). (e) Overlay of Figures (c) and (d). Figures (g–j) are the normalized intensity profile across the lines indicated in the Figures (c–f), respectively. The average power of each peak in the comb-shape spectrum on the sample is ~8 mW. The scale bar is 10 μm.

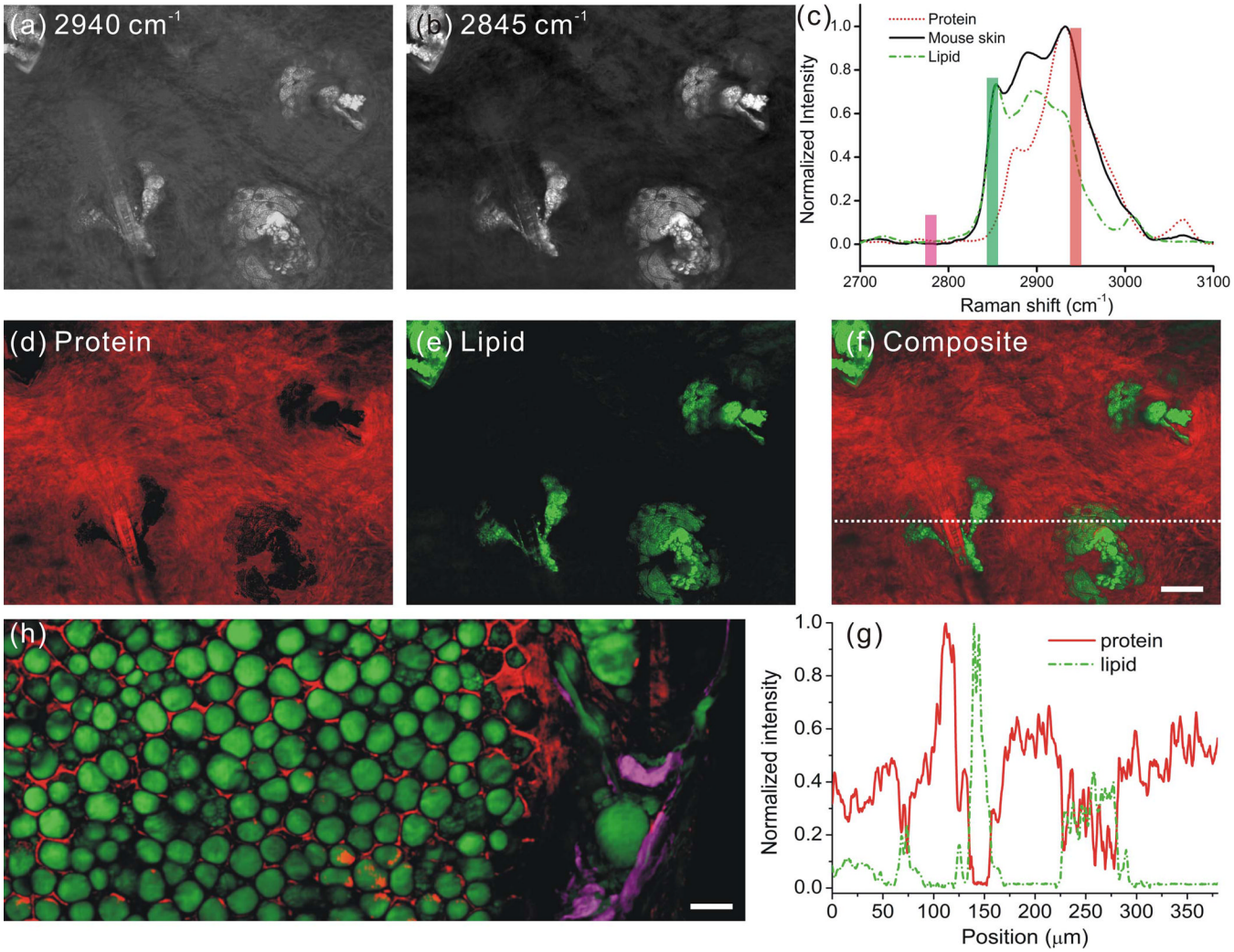


**Figure 3.**

Simultaneous two-color SRS images of the fresh mouse ear skin at (a) 2940 $cm^{-1}$ and (b) 2845 $cm^{-1}$ at the depth of ~15 μm. (c) Raman spectra of lipid, protein and the mouse skin. By calculation with the Equations (1–3), pure protein and lipid distribution could be quantitatively retrieved from the two-color images (Figures (a) and (b)), as shown in Figures (d) and (e), respectively. (f) Overlay of figures (d) and (e). (g) The intensity profile across the line indicated in Figure (f) for both protein and lipid. (h) Overlapped distribution of lipid (green), protein (red) and blood (magenta) retrieved from the simultaneous three-color images (SRS or TPA) from the same sample at the depth of ~50 μm with 2940 $cm^{-1}$, 2845 $cm^{-1}$ and 2780 $cm^{-1}$. The average power of each peak in the comb-shape spectrum on the sample is ~15 mW. The scale bar is 20 μm.